行政院國家科學委員會專題研究計畫　期中精簡報告

電解質溶液在表面覆蓋離子可穿透薄膜之微管中的流動

(2/3)

計畫類別：個別型計畫
計畫編號：NSC91-2214-E-002-006-
執行期間：91 年 08 月 01 日至 92 年 07 月 31 日
執行單位：國立臺灣大學化學工程學系暨研究所

計畫主持人：徐治平

報告類型：精簡報告

處理方式：本計畫可公開查詢

中　華　民　國 92 年 5 月 7 日

計畫執行概要

本計畫目前進展順利，已完成主要的理論推導與主控方程式的求解，將於近期內進行相關之數值模擬與分析。後附資料爲目前已獲得之部份結果。

ABSTRACT

The electrokinetic flow of an electrolyte solution in a rectangular microchannel is investigated theoretically. The present analysis extends previous results in that a two -dimensional problem is considered and the wall of the microchannel is covered by an ion-penetrable charged membrane layer; the latter simulates a biological system. The volumetric flow rate, the total electric current, the electroviscous effect, and the streaming potential of the system under consideration are evaluated. We show that the variations of these quantities as a function of the aspect ratio of the microchannel may have a local minimum or a local maximum at a medium level of ionic strength, which depends upon the thickness of the membrane layer. Some phenomena, which are predicted by the corresponding bare-wall model, may not be observed in the present case. For example, the variation of the electroviscous effect as a function of the electrokinetic radius may not have a local maximum.

1. INTRODUCTION

The flow of an electrolyte solution in a microchannel driven by an applied electric field and/or pressure gradient has wide applications in both industrial and biomedical processes. The former includes, for example, the design of micro-fluidic systems and micro-heat sinks used in electronic cooling, and the latter includes, for instance, the simulation of the flow of fluid in organic bodies and the biomedical diagnostic instruments. In contrast to the flow of fluid in a macro-channel, if the characteristic dimension of a channel reaches the micrometer size, the behavior of fluid flow inside is strongly influenced by the electrical properties of channel wall, and the corresponding equations governing the flow behavior needs to be modified accordingly. Burgreen and Nakache [1] analyzed the electrokinetic flow in an ultrafine capillary slit by extending the classic theory, which is limited to the flow in a channel of large electrokinetic radius or to a wall at low surface potentials. Rice and Whitehead [2] investigated the effect of electrokinetic radius on the behavior of the electrokinetic phenomena in a narrow cylindrical capillary at Debye-Hückel conditions. Sørensen and Koefoed [3] evaluated electrokinetic phenomenological coefficients for capillaries with a circular cross section and a bare-wall fixed charge under Debye-Hückel conditions at all ratios between pore radius and Debye length. The reciprocity relation of Onsager were derived for two dimensional flow in capillaries with any fixed cross section without regard to any specific solution for the space charge distribution using only the Poisson equation, the Navier-Stokes equation and Green's theorem. The flow of an electrolyte solution between two parallel plates, each is covered by an ion-penetrable membrane, was discussed by Donath and Voigt [4]. They showed that if the fixed charge in the membrane phase follows the distribution, which satisfies a minimum energy criterion, then the streaming current can be derived analytically [5]. Similar problem was

also examined by Ohshima and Kondo [6]. By assuming uniform fixed charge distribution, large separation between two plates, and thick membrane, they were able to derive approximate expressions for electroosmotic velocity, volumetric flow rate, total current, and the streaming potential. Tseng et al. [7] considered the flow of an electrolyte solution in a planar slit the wall of which is covered by an ion-penetrable charged membrane. An approximate analytical expression for electrical potential was derived, and the behaviors of the electrokinectic phenomena were explored. Keh and Liu [8] examined the electrokinetic flow in a capillary with circular cross section, the wall of which is covered by a charged surface layer bearing uniformly distributed fixed charge, under the conditions of low electrical potential. They showed that, depending upon the characteristics of the electrolyte solution, the surface charge, the capillary geometry, and the structure of the surface layer, either an augmented or a diminished electrokinetic flow relative to the flow in a wall-free capillary may be observed.

Most of the previous studies are dealing with a one-dimensional problem such as planar slits and cylindrical channels. Although mathematical treatment can be simplified drastically by choosing these idealized models, problems which involve a higher-dimensional description such as rectangular and elliptical channels are not uncommon in practice, and extending the analyses to these cases are highly desirable for a more realistic consideration. Yang and Li [9] examined the effects on a pressure-driven flow of an electrolyte solution in a rectangular microchannel. A two-dimensional Poisson-Boltzmann equation was solved numerically for the electrical field, and a Green-function approach was adopted to derive the solution for the flow field. They showed that the apparent viscosity strongly depends on the electrokinetic diameter, ionic concentration, and the zeta potential of the channel wall.

In the present study, the electrokinetic flow of an electrolyte solution in a

rectangular microchannel, the wall of which is covered by an ion-penetrable charged membrane, is investigated. The present discussion extends previous analyses for rigid surfaces to a more general case, and in particular, the type of the surface considered is a more realistic description for biological systems. This type of surface was justified experimentally, in which fixed charges were found to distribute in a layer of finite thickness, rather than over a surface [10]. Apparently, the conventional rigid surface models needed to be revised accordingly so that both the electric potential and the electrokinetic properties associated with this type of surfaces can be described adequately, which is of practical significance. It was found, for example, that the electrokinetic behavior is influenced significantly by the electroosmotic flow or the penetration of the surface layer through hydrodynamic flow [4,6-8].

2. THEORY

As illustrated in Fig.1, we consider a steady flow of an electrolyte solution in a rectangular microchannel, which consists of a rigid wall of thickness ξ and an ion-penetrable membrane of width d carrying uniformly distributed fixed charge. Let the width, height, and length of the microchannel be $2(W+\xi)$, $2(H+\xi)$, and L, respectively. Suppose that L is sufficiently large such that the end effect of the flow field can be neglected. The Cartesian coordinates are chosen with its origin located at the center of the microchannel, and the flow of liquid is in the z-direction. This implies that both the x- and the y-components of the fluid velocity $\mathbf{V}$ vanish, and its z-component, V_z, can be expressed as $V_z = u(x,y)$. A uniform electrical field, $\mathbf{E_z}$ with strength $E_z = -\partial\psi/\partial z$, and a uniform pressure gradient, $\mathbf{P}$, with magnitude $P = -\partial p/\partial z$, are applied in the direction of the flow of the liquid phase, ψ and p being, respectively, the electrical potential and the pressure. The permittivity and the

viscosity of the liquid phase are ε and η respectively. The symmetric nature of the problem under consideration suggests that only a quarter domain of the rectangular cross section, $x \in [0,W]$ and $y \in [0,H]$ needs to be considered.

2.1. Electrical Field

The electrical potential $\psi(x,y,z)$ comprises that due to the applied electrical field, $-E_z z$, and that due to the presence of the charged membrane layer $\phi(x,y)$. Suppose that $\psi(x,y,z)$ can be decomposed as [6]

$$\psi(x,y,z) = \phi(x,y) - E_z z \qquad (1)$$

We assume that $\phi(x,y)$ can be described by the Poisson equation [11]

$$\frac{d^2\phi}{dx^2} + \frac{d^2\phi}{dy^2} = \frac{-(\rho_{el} + jsFC_0)}{\varepsilon}, \quad 0 \le x \le W, \quad 0 \le y \le H, \qquad (2)$$

where C_0 and ρ_{el} are respectively the concentration of fixed charge and the space charge density of mobile ions, and s is the valence of fixed charge in the membrane phase. The parameter j is a region index (j=0 for liquid phase and j=1 for membrane phase). If the concentrations of ionic species in the liquid phase follow the Boltzmann distribution, then

$$\rho_{el} = aC_a^0 F[\exp(-aF\phi/RT) - \exp(bF\phi/RT)], \qquad (3)$$

where a and b are respectively the valence of cations and that of anions, C_a^0 is the

bulk concentration of cations, T is the absolute temperature, and R and F are respectively the gas constant and the Faraday constant. Eq.(2) can be rewritten in scaled form as

$$\frac{d^2\Phi}{dX^2}+\frac{d^2\Phi}{dY^2}=K^2\,\frac{G+jN}{a+b},\ \ 0\le X\le W/D_h,\ \ 0\le Y\le H/D_h. \qquad (4)$$

In these expressions, $\Phi = F\phi/RT$, $N=-sC_0/aC_a^0=-(a+b)sC_0/2I$, $I=a(a+b)C_a^0/2$, $G=exp(b\Phi)-exp(-a\Phi)$, $X=x/D_h$, $Y=y/D_h$, and $K=kD_h$, where I is the ionic strength, $D_h=4WH/(W+H)$ is the hydraulic diameter of the rectangular microchannel, and the Debye-Huckel parameter k is defined by

$$k=\left(\frac{aC_a^0(a+b)F^2}{\varepsilon RT}\right)^{1/2}=\left(\frac{2IF^2}{\varepsilon RT}\right)^{1/2} \qquad (5)$$

The boundary conditions associated with Eq.(4) are assumed as

$\overline{\nabla}\Phi\bullet\bar{n}=0$, X=0 or Y= 0

$$\Phi\big|_{\Omega^+}=\Phi\big|_{\Omega^-}$$

$$\overline{\nabla}\Phi\bullet\bar{n}\big|_{\Omega^+}=\overline{\nabla}\Phi\bullet\bar{n}\big|_{\Omega^-}$$

(6c)

$\overline{\nabla}\Phi \bullet \bar{n} = 0$, $X=W/D_h$ or $Y=H/D_h$ (6c)

In these expressions $\overline{\nabla}$ is the gradient operator and $\bar{n}$ is the unit normal vector at interface. Eq.(6a) arises from the symmetric nature of the problem under consideration. Eqs.(6b) and (6c) state that both the electrical potential and the electric field are continuous at the liquid-membrane interface (Ω^+ denotes the liquid side and Ω^- represents the membrane side). Note that, to account for the difference between the permittivity of the membrane phase and that of the solution phase, a correction factor should be added to either side of Eq.(6c). For simplicity, we assume that this factor is unity. This is appropriate if the porosity of the membrane phase is large. Eq.(6d) implies that there is no electric field at the rigid wall of the microchannel, which is satisfied if there is complete electroneutrality in the microchannel, or if the conductivity in the external wall is very high.

2.2. Flow Field

Suppose that the liquid phase is incompressible, and that the axial variation of its velocity *u(x,y)* can be described by the modified Navier-Stokes equation [6,12]

$$\frac{d^2u}{dx^2}+\frac{d^2u}{dy^2}=-\frac{[-(dp/dz)+\rho_{el}E_z-j\gamma u]}{\eta},\ 0\le x\le W,\ \ 0\le y\le H \qquad (7)$$

where γ is the friction coefficient per unit volume of the membrane layer. Note that the effect of gravity is neglected in Eq.(7) and a body force term $\rho_{el}E_z$ is included. Eq.(7) can be rewritten in scaled form as

$$\frac{\partial^2 U}{\partial X^2}+\frac{\partial^2 U}{\partial Y^2}=K^2\left[L\frac{G}{a+b}-M+j\lambda^2 U\right],\ 0\le X\le W/D_h,\ 0\le Y\le H/D_h \quad (8)$$

where $U=u/u_0$, $L=\varepsilon RTE_z/\eta F u_0$, $\lambda^2=\gamma/\eta k^2$, and $M=P/\eta k^2 u_0$, u_0 being a reference velocity. The boundary conditions associated with Eq.(8) are assumed as

$$\bar{\nabla}U\bullet\bar{n}=0,\ X=0 \text{ or } Y=0 \quad (9$$

$$U\big|_{\Omega^+}=U\big|_{\Omega^-} \quad (9b)$$

$$\bar{\nabla}U\bullet\bar{n}\big|_{\Omega^+}=\bar{\nabla}U\bullet\bar{n}\big|_{\Omega^-} \quad (9$$

$$U=0,\ X=W/D_h \text{ or } Y=H/D_h \quad (9d$$

Eq.(9a) arises from the symmetric nature of the problem under consideration. Eqs.(9b) and (9c) state the continuity conditions of velocity and shear stress. Here, we assume that the viscosity of the liquid in the membrane phase is the same as that in the solution phase. As pointed out by Masliyah et al. [13], if the porosity of the membrane phase is sufficiently high, Eq.(9c) is satisfactory. Eq.(9d) states the no-slip condition at the rigid wall of the microchannel.

2.3. Volumetric Flow Rate and Eelectric Current

When an electrolyte solution is forced through a microchannel under an applied electric field, the counterions in the mobile part of the electrical double layer are driven to some end of the microchannel, depend on which direction the electric

field applied. These moving counterions will pull the surrounding liquid molecules with them and cause a volume flow through the microchannel. Apparently, the coions in the electrical double layer will also cause an opposite flow. However, the concentration of counterions in the electrical double layer is always higher than that of coions, this will cause a net volume flow in the moving direction of counterions. The volumetric flow rate, V_t, contributed by electroosmosis, through the rectangular microchannel is given by

$$V_t = 4\int_0^H \int_0^W u\, dx\, dy$$

where u is evaluated at E_z and P=0. From the description above, the electrolyte ions are driven by the applied electric field to the opposite direction, depend on the sign of charge they carried. These moving charged ions will cause a electric current, no matter which kinds of ions, cations or anions, all provide the positive contribution to the electric current. The density of electric current, $i(x,y)$, can be evaluated by

$$i(x,y) = aFC_a v_a - bFC_b v_b \qquad (11)$$

where C_a and C_b are respectively the concentrations of cations and anions, and v_a and v_b are the velocities of cations and anions respectively. The electrochemical potentials of cations and anions, μ_a and μ_b, can be expressed respectively as [6]

$$\mu_a(x,y,z) = \mu_{a0} + ae\psi(x,y,z) + k_B T \ln[C_a(x,y)] \qquad (12a)$$

and

$$\mu_b(x,y,z) = \mu_{b0} - be\psi(x,y,z) + k_B T \ln[C_b(x,y)] \qquad (12b)$$

where μ_{a0} and μ_{b0} are constant, e is the elementary charge, and k_B is the Boltzmann constant. The velocity of ion species m can be expressed as [6]

$$v_m(x,y) = u(x,y) - \frac{1}{f_m}\frac{\partial}{\partial z}\mu_m \qquad (1$$

where f_m is the drag coefficient of ionic species m, $m=a,b$. Substituting this expression into Eqs.(12a) and (12b), and substituting the resultant expressions into Eq.(11), we have

$$i(x,y) = \rho_{el}u(x,y) + \frac{F^2 E_z}{N_0}\left[\frac{a^2}{f_a}C_a(x,y) + \frac{b^2}{f_b}C_b(x,y)\right] \qquad (14a)$$

This expression can be rewritten in terms of scaled quantities as

$$i(X,Y) = \frac{FsC_0}{N}\left\{-Gu_0 U + \frac{FE_z}{N_0}\left[\frac{a}{f_a}exp(-a\Phi) + \frac{b}{f_b}exp(b\Phi)\right]\right\} \qquad (14b)$$

where N_0 denotes the Avogadro's number. The total electric current in the z-direction, I_t, can be evaluated by

$$I_t = 4\int_0^H\int_0^W i(x,y)\,dx\,dy = 4D_h^2\int_0^{H/D_h}\int_0^{W/D_h} i(X,Y)\,dX\,dY \qquad (15)$$

2.4. Streaming Potential and Electroviscous Effect

When a liquid is forced through a microchannel under a hydrostatic pressure difference, the ions in the mobile part of the electrical double layer are carried toward the downstream end. The accumulation of ions downstream sets up an induced electric field. When a steady state is reached, the total net electrical current, I_t, should be zero. The induced electric field at that moment is called streaming potential E_{st}. Eqs.(14) and (15) lead to

$$E_{st} = \left(\int_0^{H/D_h} \int_0^{W/D_h} G u_0 U \, dX \, dY \right) \Bigg/ \left(\int_0^{H/D_h} \int_0^{W/D_h} \frac{F}{N_0} \left[\frac{a}{f_a} exp(-a\Phi) + \frac{b}{f_b} exp(b\Phi) \right] dX \, dY \right) \tag{16}$$

Note that this is an implicit expression. The streaming potential will drive counterions to move in the opposite direction to the direction of the pressure-driven flow when electrical double layer is present in a microchannel. The moving counterions also pull the surrounding liquid molecules with them and reduce the volumetric flow in the forward direction. The apparent viscosity of the liquid, η_a, is higher than the corresponding flow when the electrical double layer is absent, η, the so-called electroviscous effect. Define R_{vis} as the ratio

$$R_{vis} \equiv \frac{\eta_a}{\eta}$$

The value of η_a can be estimated by first substituting $E_z = E_{st}$ into Eq.(7) and solving the resultant expression for u. Eq.(10) is then used under the condition $E_z = E_{st}$ and

$P=-\partial p/\partial z$ to evaluate volumetric flow rate V_{t1}. This procedure is repeated again with $\rho_{el}=0$ and $\eta=\eta_a$ in Eq.(7). The volumetric flow rate thus obtained is denoted as V_{t2}, and η_a can be evaluated by equating $V_{t1}=V_{t2}$.

3. RESULTS AND DISCUSSIONS

The governing equations, Eqs.(4) and (8), are solved numerically subject to Eqs.(6) and (9) by PDEaseII, and the results are used to evaluate the streaming potential, the volumetric flow rate, the electric current, and the apparent viscosity by Eqs.(16), (10), (15), and (17) respectively. For illustration, we consider a 1:1 electrolyte solution, and the valence of fixed charge is chosen as -1. The value of γ in Eq.(7) can be estimated by the modified Rouse theory [14]. In the case of poly(dimethyl siloxane), for example, γ is on the order of 10^{13} N•s/m^4. The experimental results reported by Mala et al. [15] indicate that the zeta potential is in the range 100 to 200 mV, and the ionic concentration varies from 10^{-4} to 10^{-6} M. Therefore, the amount of fixed charge per unit length of membrane, Q_c/Fs, is chosen as 10^{-12} C/m. The drag coefficient of cations and that of anions are assumed to be the same and has the value $f_a=f_b=10^{-12}$ kg/s [12].

Fig.2 shows the spatial variation of the scaled electrical potential in a microchannel at various combinations of the thickness of membrane d and the aspect ratio H/W. Due to the symmetric nature of the problem under consideration, only the results for a quarter channel are presented. Here, both the amount of fixed charge per unit length Q_c/Fs and the hydraulic diameter D_h are kept constant. A comparison between Fig.2a and 2b reveals that the thinner the membrane the lower the electrical potential on the wall of a microchannel. A comparison between Fig.2a and 2c suggests that the smaller the aspect ratio the higher the electrical potential on the wall of a microchannel.

Fig.3 illustrates the variations of the scaled velocity U in a microchannel at various combinations of the aspect ratio H/W and the thickness of membrane d. For comparison, the corresponding result for the case the electrical double layer is absent is also shown. Fig.3a and 3b reveals that the present of electrical double layer has the effect of reducing the liquid velocity. This is expected since the electroviscous effects. Figs.3b and 3c suggest that, for a constant hydraulic diameter D_h, the smaller the aspect ratio, the slower the flow of the liquid phase. This is because if D_h remains constant, the smaller the H/W, the narrower a microchannel, and the stronger the wall effects on the liquid flow, which leads to a smaller U. A comparison between Figs.3b and 3d reveals that the thinner the membrane the faster the flow of the liquid phase as expected.

The variations in the total electric current I_t as functions of the aspect ratio H/W at various combinations of the ionic strength I and the thickness of membrane d are presented in Fig.4. As can be seen from this figure, for a constant H/W, I_t increases with the increase in I, but decreases with the increase in d. The former is because that the larger the I the higher the concentrations of both coions and counterions in the liquid phase which has a positive effect on the total current. Although a larger I means a thinner double layer, the contribution of the ions in a double layer to the total current is limited due to the resistance of membrane. That is, the contribution to the total current by the ions in the bulk liquid phase is more significant than that by the ions in the double layer. The total resistance provided by a membrane decreases with the decrease in d, that is, the thinner the membrane the easier for ions to be driven to the downstream of a microchannel. Also, for the same ionic strength, it is more likely that the double layer of a system with a thinner membrane exceeds membrane thickness than a system with a thicker membrane. That is, it is more possible that the amount of ions outside the membrane phase for the former is greater

than that of the latter, and, therefore, the thinner the membrane, the larger the total current. Fig.4a reveals that, if I is sufficiently high, I_t increase with the decrease in H/W. On the other hand, if I is low, I_t increases with the increase in H/W, as is illustrated in Fig.4c. It is interesting to note that for a medium value of I, I_t exhibits a local minimum as H/W varies, as can be seen in Fig.4b. This local minimum disappears, however, if d is too large. The value of H/W at which the local minimum occurs increases with the increase in d. This can be elaborated as follows. For a constant hydraulic diameter D_h, the smaller the H/W the narrower a microchannel, and the shorter the height of the microchannel. In this case, the wall effect becomes more significant, that is, the viscous effect is pronounced. On the other hand, the cross sectional area of a microchannel increases with the decrease in H/W, which implies that more ions can be contained in a microchannel. If I is high, the concentration of ions in the liquid phase is high. The effect of the increase in cross sectional area is more significant than the viscous effect, and I_t increases with the decrease in H/W. On the other hand, if I is low, the concentration of ions in the liquid phase is low, and the effect of the increase in cross sectional area is less significant than the viscous effect, and I_t increases with the increase in H/W. For a medium value of I if H/W is large, the viscous effect is more important than the effect of the increase in cross sectional area, and the reverse is true if H/W is small. Therefore, I_t has a local minimum as H/W varies. Due to the fact that the smaller the d the less the resistance provided by the membrane phase, the value of H/W at which the local minimum occurs increases with the increases in d. Fig.4 also illustrates the results based on the model of Ohshima and Kondo [6] for the case of a planar slit, and those based on the linearized version of Eq.(4), i.e., under the conditions of low electrical potential (Debye-Huckel approximation). Fig.4a reveals that, if H/W is small, the present result can be approximated by that based on Ohshima and Kondo's

model. This is because if H/W is small, a microchannel becomes flat and narrow, and the presence of its left and right walls is less significant, that is, it can be approximated by a planar slit. However, as can be seen in Fig.4b and 4c, if I is low, the difference between the present result and that based on Ohshima and Kondo's model becomes appreciable, even if H/W is small. This is because the latter assumes that $2H >> d \geq 1/k$, and this condition is not satisfied if I is low. Fig.4a suggests that, if I is sufficiently high, the result based on the Debye-Hückel approximation is satisfactory. As can be seen in Fig.4b, however, if I is low, using the linearized version of Eq.(4) will lead to a significant deviation. This is because the lower the I, the higher the absolute potential on the wall of a microchannel, as can be seen in Table 1.

Figure 5 illustrates the variations in the volumetric flow rate V_t as a function of the aspect ratio H/W at various ionic strength I and thickness of membrane d. As can be seen from this figure, for a constant H/W, V_t increases with the decrease in both I and d. This is because the lower the I the thicker the double layer, and the more the amount of counterions in the double layer which can be driven by the applied electric field. In this case the volumetric flow rate needs to be large due to the drag of the solution molecules by the counterions in the double layer. When d decreases, the resistance provided by the membrane decreases accordingly, and it is easier for ions and solution molecules to be transported to the downstream of a microchannel. As pointed out in the discussion of Fig.4, for the same ionic strength, it is more likely that the amount of counterions outside the membrane phase of a system with a thinner membrane is greater than that for a system with a thicker membrane. Therefore, the volumetric flow rate of the former is greater than that of the latter. Fig.5a reveals that if I is high, V_t decreases with the increase in H/W for the case d is small, and it increases with the increase in H/W if d is large. As can be seen from Fig.5c, if I is

low, V_t decreases with the increase in H/W regardless of the thickness of membrane. Fig.5b suggests that for a medium level of I, the variation of V_t as a function of H/W may have a local maximum if the membrane is sufficiently thick. This can be elaborated as follows. If I is high, almost all the counterions in the double layer are distributed in the neighborhood of the wall of a microchannel. This implies that the effect of the interaction between the double layers near the upper and lower surfaces of the microchannel is insignificant. Also, as in the discussion of Fig.4, the effect of the increase in cross sectional area is less significant than the viscous effect, and therefore, V_t increases with the increase in H/W. However, if d is small, the former becomes more important than the latter, and V_t decreases with the increase in H/W. If I is low, the counterions in the double layer are distributed in a region far away from the wall of a microchannel, and the effect of the interaction between the double layers near the upper and the lower surfaces of the microchannel is significant. The combined effect of the interaction between the double layers near the upper and the lower surfaces of the microchannel, and the increase of the cross sectional area of the microchannel is more important than the viscous effect. Therefore V_t increases with the decrease in H/W. The qualitative behavior of Fig.5b arises from the competition of these three effects. If d is sufficiently large, the viscous effect is more significant if H/W is small, and therefore V_t increases with the increase in H/W if it is small, and the reverse is true if H/W becomes large. This leads to a local maximum of V_t as H/W varies. The value of H/W at which this local maximum occurs decreases with the decrease in d. If d is sufficiently small, the local maximum may disappear.

Figs.6 and 7 illustrate respectively the variations in the streaming potential E_{st} and the parameter R_{vis}, which characterizes the electroviscous effect, as a function of the aspect ratio H/W at various ionic strength I and thickness of membrane d. As can

be seen from Fig.6, for a fixed H/W, $|E_{st}|$ increases with the decrease in both I and d. This is because the lower the I the thicker the double layer, which implies that more amount of counterions in the double layer can be driven by the applied pressure gradient. In this case, the induced electric field is stronger, and the electroviscous effect is more significant. If the total amount of fixed charge in the membrane phase is fixed, the resistance provided by it decreases with the decrease in d, and a more amount of liquid phase needed to be driven to the downstream of the microchannel. Also, for the same ionic strength, it is more possible that the amount of counterions outside the membrane phase for the former is greater than that of the latter. Both of these two factors will result in an increase in both $|E_{st}|$ and R_{vis}. Fig.6a and Fig.7a suggest that if I is high, both $|E_{st}|$ and R_{vis} increase with the increase in H/W, and the reverse is true if I is low, as shown in Fig.6c and Fig.7c. As illustrated in Fig.6b and Fig.7b, for a medium level of I, the variation of both $|E_{st}|$ and R_{vis} as a function of H/W exhibits a local maximum. The value of H/W at which the local maximum occurs increases with the increase in d. This can be explained by the same reasons as those stated in the discussion of Fig.5b.

Fig.8 shows the variation of R_{vis} as a function of the electrokinetic diameter D_e ($= kD_h$) at various aspect ratio H/W and hydraulic diameter D_h. This figure reveals that if $D_e \to \infty$, which implies that the double layer becomes infinitely thin (for a fixed D_h), R_{vis} approaches unity. That is, the interaction between the double layers near the upper and the lower surfaces of the microchannel becomes negligible, and the electroviscous effect disappears. Fig.8 also suggests that if $D_e \to 0$, R_{vis} approaches to a constant. It is interesting to note that the influence of D_h on the behavior of R_{vis} vs D_e curve is important, which has been overlooked in most of the results reported in

the literature. As concluded by Burgreen and Nakache [1], Rice and Whitehead [2], and Yang and Li [9], for slit, cylindrical tube, and rectangular microchannel, respectively, the variation of R_{vis} as a function of D_e has a local maximum. Here, we show that this local maximum may not be present for a rectangular microchannel covered by a membrane layer. As pointed out by Burgreen and Nakache [1], if the zeta potential is sufficiently high, the local maximum of R_{vis} vs D_e curve will disappear. As shown in Table 1, in our case since the absolute potential on the wall of a microchannel increases with the decrease in D_e, the local maximum may disappear if D_e is too small.

According to Sørensen and Koefood [3], regardless of the kind of cross section and the type of fixed charge distribution, Onsager relation needs to be satisfied. For illustration, this is examined for the relation

$$\left(\frac{V_t}{I_t}\right)_{P=0} = \left(\frac{E_{st}}{P}\right)_{I_t=0}$$

Fig.9 shows the variation of $(V_t/I_t)_{P=0}$ as a function of $(E_{st}/P)_{It=0}$ at various aspect ratio H/W. As can be seen from this figure, the Onsager relation is justified.

The variation of the total current I_t as a function of the aspect ratio H/W at various ionic strength I and membrane thickness d is illustrated in Fig.10. Both the cross sectional area of a microchannel and that of the membrane layer are held fixed in each curve. For convenience, a cylindrical channel of diameter D_{hc} covered by a circular membrane of thickness d_c is adopted as a basis. Fig.10 shows I_t that increases with the increase in H/W at each level of I. This is because if the cross sectional area of a microchannel is fixed, the smaller H/W, the smaller the separation distance between the top and the bottom walls of a microchannel. In this

case, both the hydrodynamic viscous and the double layer interactions between these two walls are more significant, which leads to a smaller total current. Fig.10 also shows that I_t decreases with the increase in the thickness of membrane layer, as expected.

REFERENCES

[1] Burgreen, D., and Nakache, F.R., *J. Phys. Chem.* **68**, 1084 **(**1964**)**.

[2] Rice, C.L., and Whitehead, R., *J. Phys. Chem.* **69**, 4017 (1965).

[3] Sørensen, T.S., and Koefoed, J., *J. Chem. Soc. Faraday Trans. II* **70**, 665 (1974**)**.

[4] Donath, E., and Voigt, A., *J. Colloid Interface Sci.* **109**, 122 (1986).

[5] Donath, E., and Voigt, A., *J. Theor. Biol.* **101**, 569 (1983).

[6] Ohshima, H., and Kondo, T., *J. Colloid Interface Sci.* **135**, 443 (1990).

[7] Tseng, S., Kao, C.Y., and Hsu, J.P., *Electrophoresis* **21**, 3541 (2000).

[8] Keh, H.J., and Liu, Y.C., *J. Colloid Interface Sci.* **172**, 222 (1995).

[9] Yang, C., and Li, D., *J. Colloid Interface Sci.* **194**, 95 (1997).

[10] Hunter, R.J., "Zeta potential in Colloid Science. Principles and Applications," Academic Press: New York, 1981.

[11] Hunter, R.J., "Foundations of Colloid Science," Vol. 1; Oxford University Press: Oxford, 1989.

[12] Van de Ven, T.G.M., "Colloidal Hydrodynamic." Academic Press: New York, 1989.

[13] Masliyah, J.H., Neale, G., Malysa, K., and Van de Ven, T.G.M., *Chem. Eng. Sci.* **42**, 245 (1987).

[14] Ferry, J.D., "Viscoelastic Properties of Polymers", 3rd ed.; Wiley, New York, 1980.

[15] Mala, G.M., Li, D., Werner, C., Jacobasch, H.J., and Ning, Y.B., *Int. J. Heat and Fluid Flow* **18**, 489 (1997).

Table 1 Variation of absolute electrical potential on the wall of microchannel, $|\Phi_W|$, for various electrokinetic radius D_e and ionic strength I. The hydraulic diameter D_h is fixed at 10^{-6} m. The parameters used are $a=b=1$, $s=-1$, $T=298$ K, $Q_c/Fs=10^{-12}$ C/m, $\varepsilon=7.08\text{x}10^{-10}$ C/V.m, $H/W=1$, and $d=D_h/10$.

I(M)	10^{-3}	10^{-4}	10^{-5}	10^{-6}	10^{-7}	10^{-8}	10^{-9}
D_e	$1.030\text{x}10^{2}$	$3.257\text{x}10^{1}$	$1.030\text{x}10^{1}$	3.257	1.030	$3.257\text{x}10^{-1}$	$1.030\text{x}10^{-1}$
$\lvert\Phi_W\rvert$	1.132	3.326	5.627	7.930	$1.023\text{x}10^{1}$	$1.253\text{x}10^{1}$	$1.484\text{x}10^{1}$

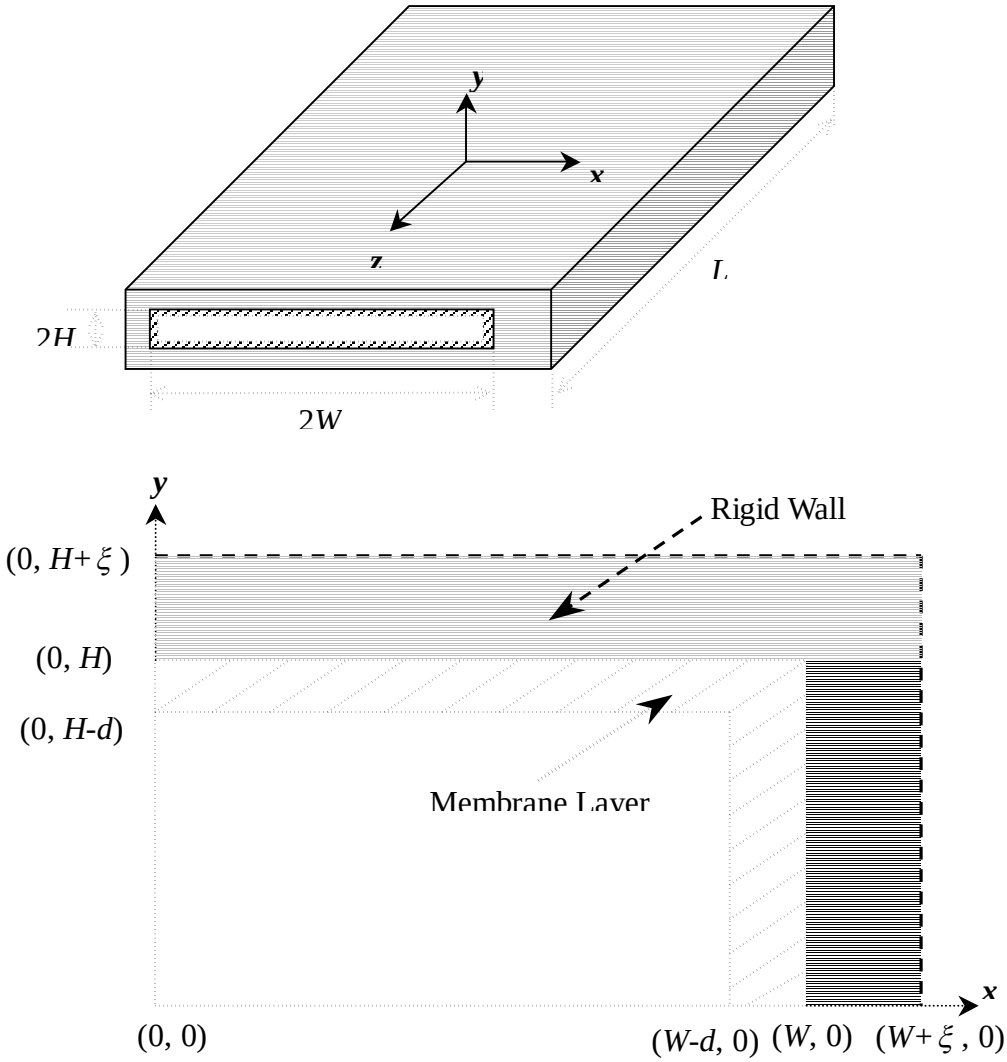

Fig.1. Schematic representation of the system under consideration. A rectangular microchannel consists of a rigid wall of thickness ξ, which is covered by an ion-penetrable membrane of thickness d. L, $2(H+\xi)$, and $2(W+\xi)$ are the length,

the height, and the width of the microchannel, respectively.

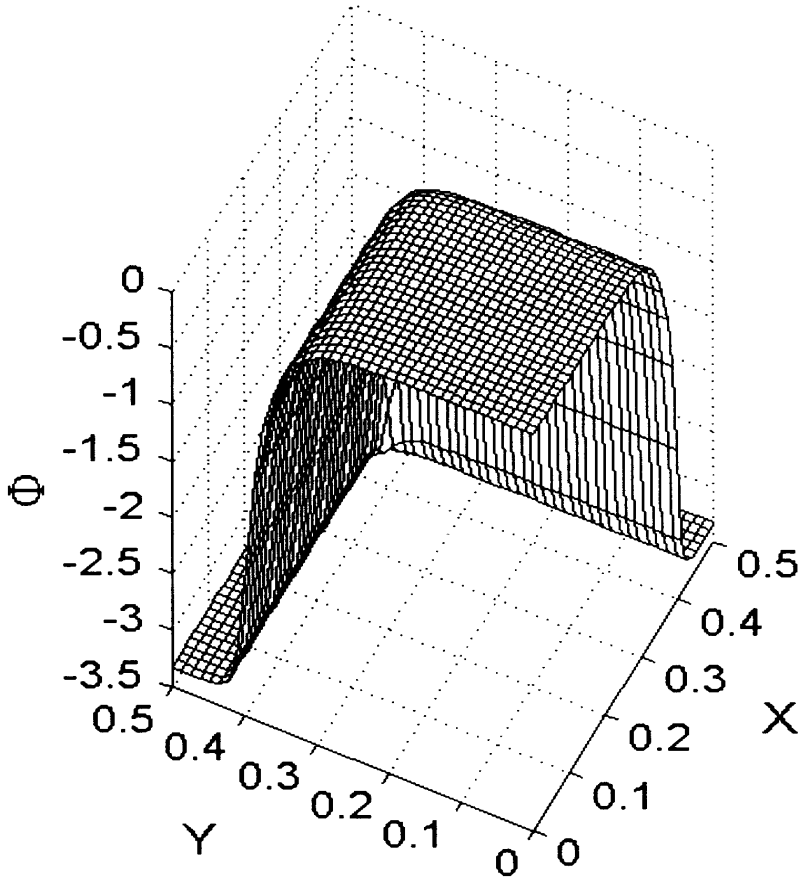

Fig.2a. Variation of scaled potential Φ in a microchannel at various combinations of aspect ratio H/W and membrane thickness d. Parameters used are $D_h=10^{-6}$ m, $I=10^{-4}$ M, $a=b=1$, $s=-1$, $T=298$ K, $Q_c/Fs=10^{-12}$ C/m, $\varepsilon=7.08\text{x}10^{-10}$ C/V.m. ($H/W=1$ and $d=D_h/10$).

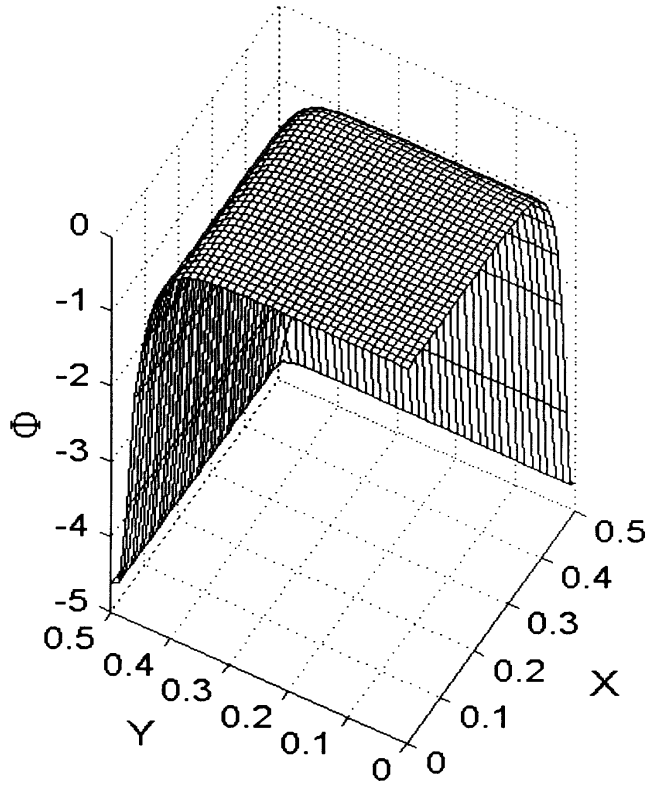

Fig.2b. Variation of scaled potential Φ in a microchannel at various combinations of aspect ratio H/W and membrane thickness d. Parameters used are $D_h=10^{-6}$ m, $I=10^{-4}$ M, $a=b=1$, $s=-1$, $T=298$ K, $Q_c/Fs=10^{-12}$ C/m, $\varepsilon=7.08\text{x}10^{-10}$ C/V.m. ($H/W=1$ and $d=D_h/40$).

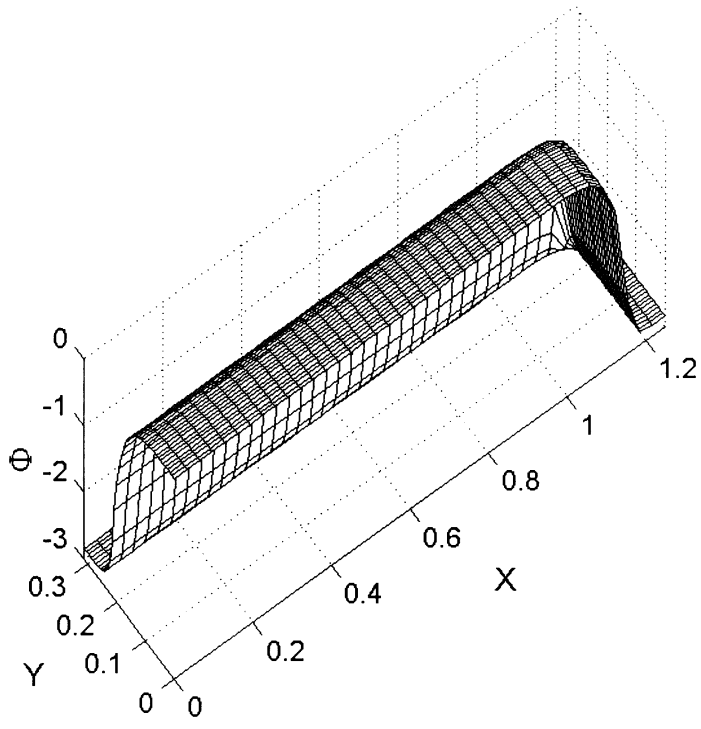

Fig.2c. Variation of scaled potential Φ in a microchannel at various combinations of aspect ratio H/W and membrane thickness d. Parameters used are $D_h=10^{-6}$ m, $I=10^{-4}$ M, $a=b=1$, $s=-1$, $T=298$ K, $Q_c/Fs=10^{-12}$ C/m, ε =7.08x10^{-10} C/V.m. ($H/W=1/4$ and $d=D_h/10$).

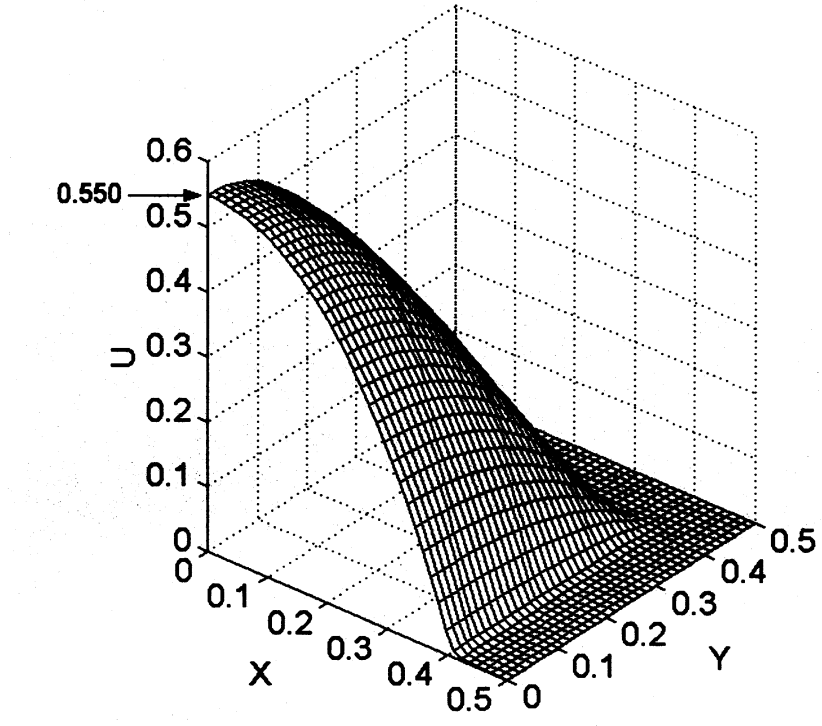

Fig.3a. Variation of scaled velocity U in a microchannel at various combinations of aspect ratio H/W and membrane thickness d. Parameters used are $D_h=10^{-6}$ m, $I=10^{-4}$ M, and $P=10^{7}$ N/m^3, $u_0=10^{-3}$m/s. Key: $a=b=1$, s=–1, $T=298$ K, $Q_c/Fs=10^{-12}$ C/m, $\varepsilon=7.08\text{x}10^{-10}$ C/V.m, $\gamma=10^{13}$ N.s/m^4, $\eta=9\text{x}10^{-4}$ kg/m.s, $f_a=f_b=10^{-12}$ kg/s (without double layer; $H/W=1$ and $d=D_h/10$).

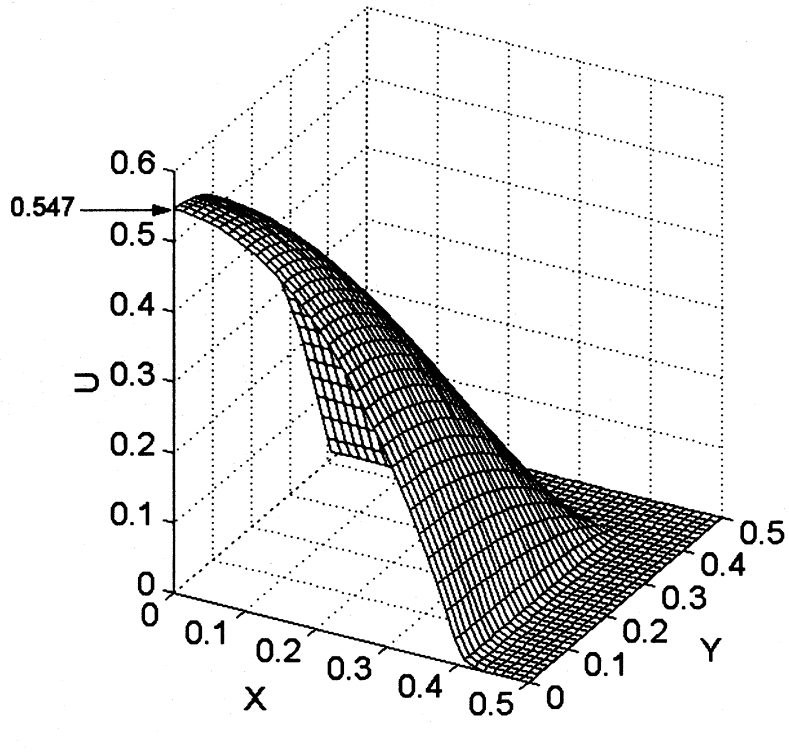

Fig.3b. Variation of scaled velocity U in a microchannel at various combinations of aspect ratio H/W and membrane thickness d. Parameters used are $D_h=10^{-6}$ m, $I=10^{-4}$ M, and $P=10^{7}$ N/m^3, $u_0=10^{-3}$m/s. Key: $a=b=1$, s=–1, $T=298$ K, $Q_c/Fs=10^{-12}$ C/m, ε =7.08x10^{-10} C/V.m, γ =10^{13} N.s/m^4, η =9x10^{-4} kg/m.s, $f_a=f_b=10^{-12}$ kg/s (with double layer; H/W=1 and $d=D_h/10$).

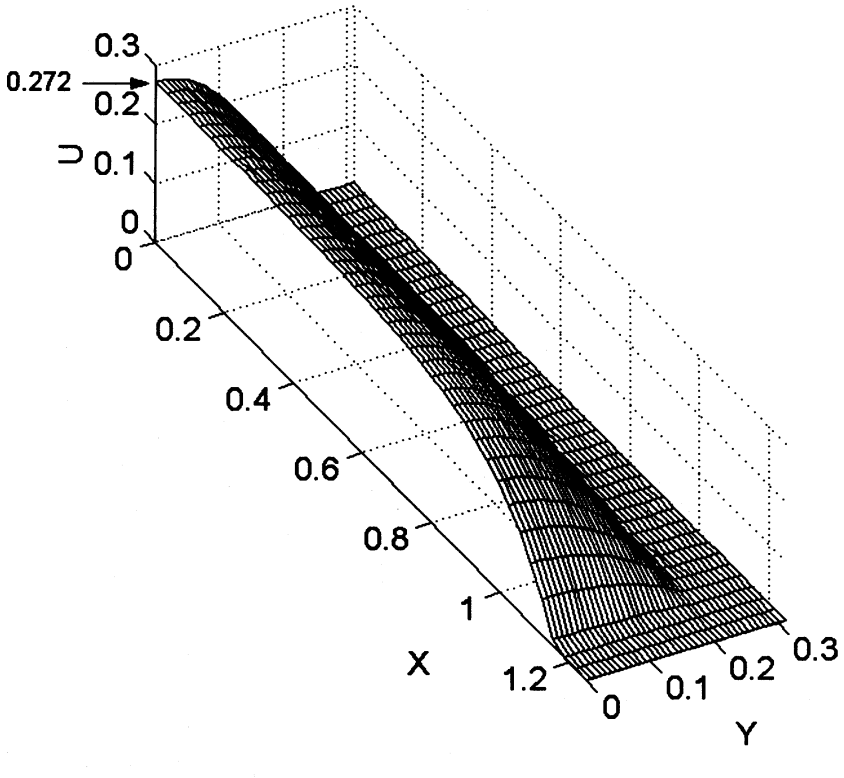

Fig.3c. Variation of scaled velocity U in a microchannel at various combinations of aspect ratio H/W and membrane thickness d. Parameters used are $D_h=10^{-6}$ m, $I=10^{-4}$ M, and $P=10^{7}$ N/m^3, $u_0=10^{-3}$m/s. Key: $a=b=1$, s=-1, $T=298$ K, $Q_c/Fs=10^{-12}$ C/m, ε =7.08x10^{-10} C/V.m, γ =10^{13} N.s/m^4, η =9x10^{-4} kg/m.s, $f_a=f_b=10^{-12}$ kg/s (with double layer; H/W=1/4 and $d=D_h/10$).

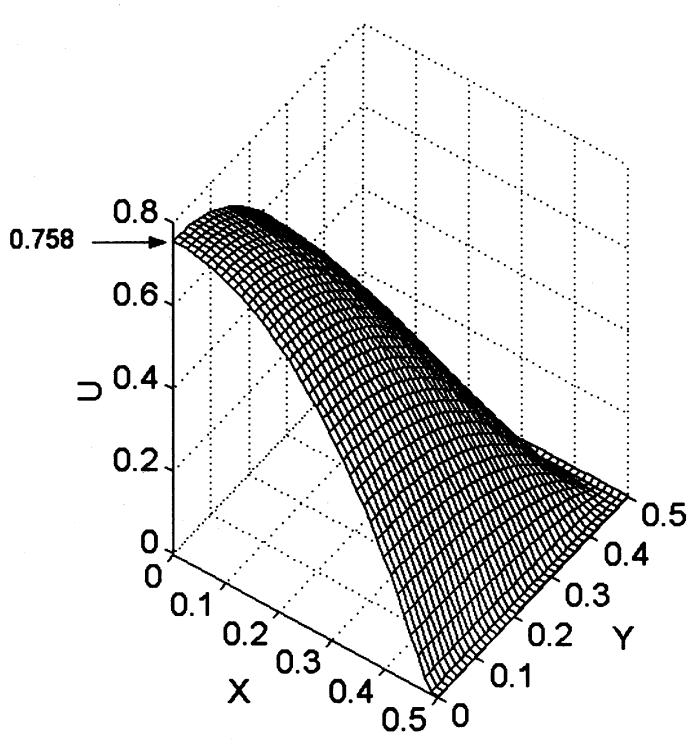

Fig.3d. Variation of scaled velocity U in a microchannel at various combinations of aspect ratio H/W and membrane thickness d. Parameters used are $D_h=10^{-6}$ m, $I=10^{-4}$ M, and $P=10^{7}$ N/m^3, $u_0=10^{-3}$m/s. Key: $a=b=1$, s=–1, $T=298$ K, $Q_c/Fs=10^{-12}$ C/m, ε =7.08x10^{-10} C/V.m, γ =10^{13} N.s/m^4, η =9x10^{-4} kg/m.s, $f_a=f_b=10^{-12}$ kg/s (with double layer; $H/W=1$ and $d=D_h/40$).

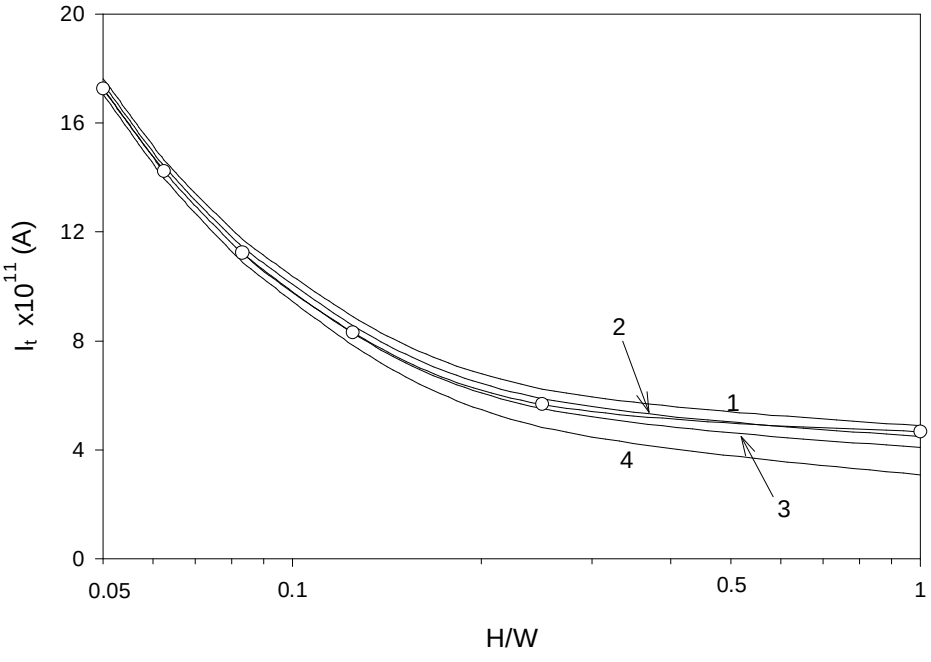

Fig.4a. Variation of total current I_t as a function of aspect ratio H/W at various ionic strength I and membrane thickness d for the case D_h=10^{-6} m, E_z=1000 V/m and P=0 N/m^3. Curve 1, $d=D_h/40$; Curve 2, $d=D_h/20$; Curve 3, $d=D_h/10$; Curve 4 is the result based on Ohshima and Kondo's model [6], and symbol o represents that based on Debye-Huckel approximation for the case $d=D_h/10$. Key: same as Fig.3 (I=10^{-3} M).

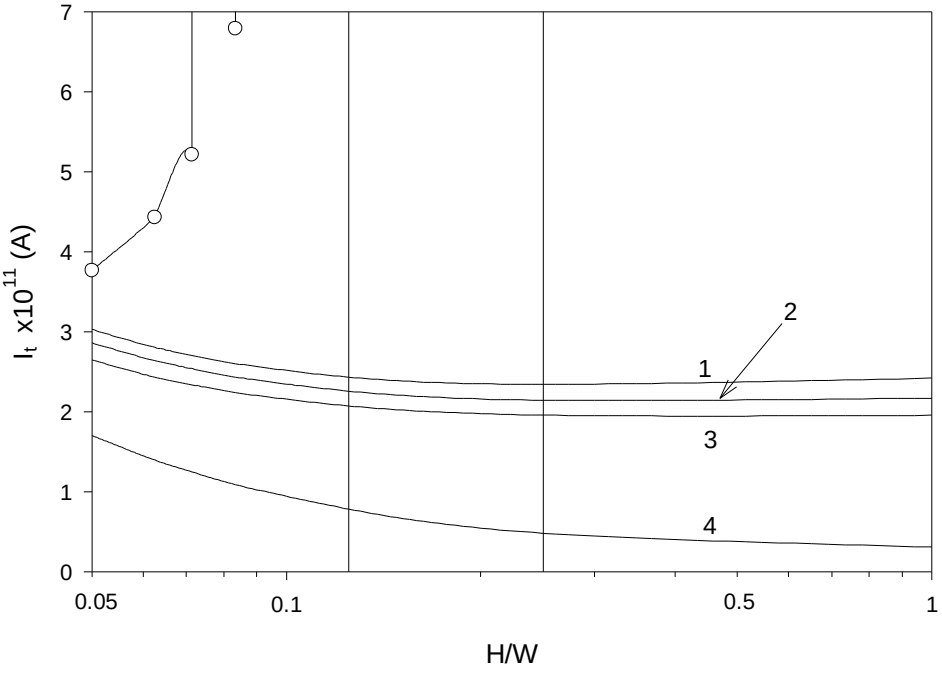

Fig.4b. Variation of total current I_t as a function of aspect ratio H/W at various ionic strength I and membrane thickness d for the case D_h=10^{-6} m, E_z=1000 V/m and P=0 N/m^3. Curve 1, $d=D_h/40$; Curve 2, $d=D_h/20$; Curve 3, $d=D_h/10$; Curve 4 is the result based on Ohshima and Kondo's model [6], and symbol o represents that based on Debye-Huckel approximation for the case $d=D_h/10$. Key: same as Fig.3 (I=10^{-4} M).

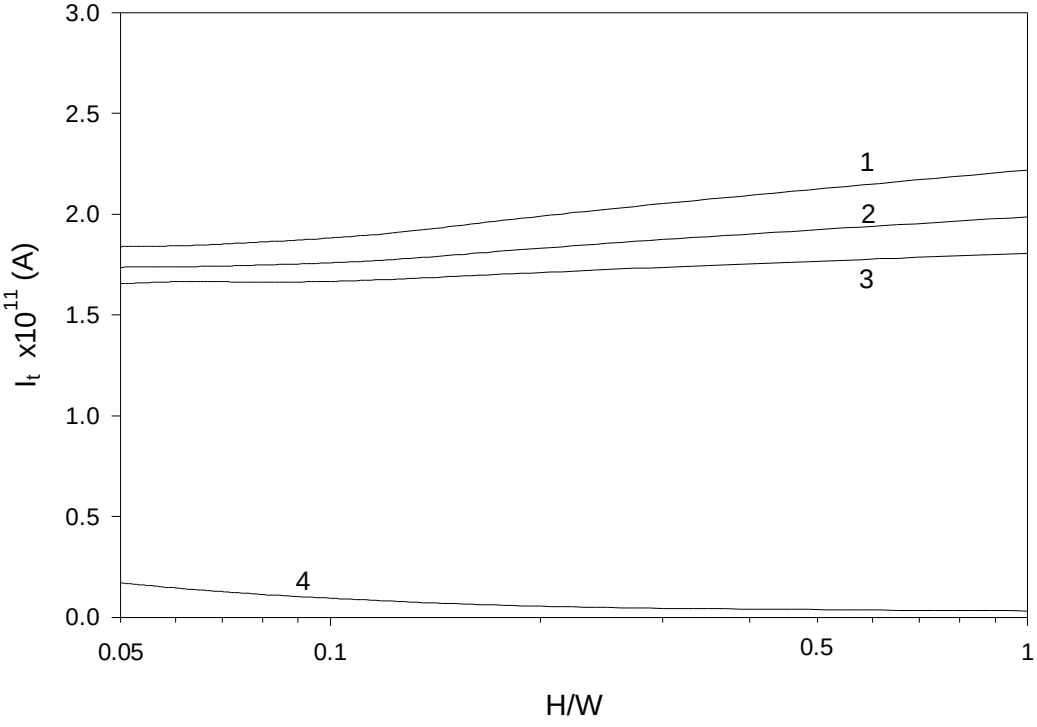

Fig.4c. Variation of total current I_t as a function of aspect ratio H/W at various ionic strength I and membrane thickness d for the case D_h=10^{-6} m, E_z=1000 V/m and P=0 N/m^3. Curve 1, $d=D_h/40$; Curve 2, $d=D_h/20$; Curve 3, $d=D_h/10$; Curve 4 is the result based on Ohshima and Kondo's model [6], and symbol o represents that based on Debye-Huckel approximation for the case $d=D_h/10$. Key: same as Fig.3 (I=10^{-5} M).

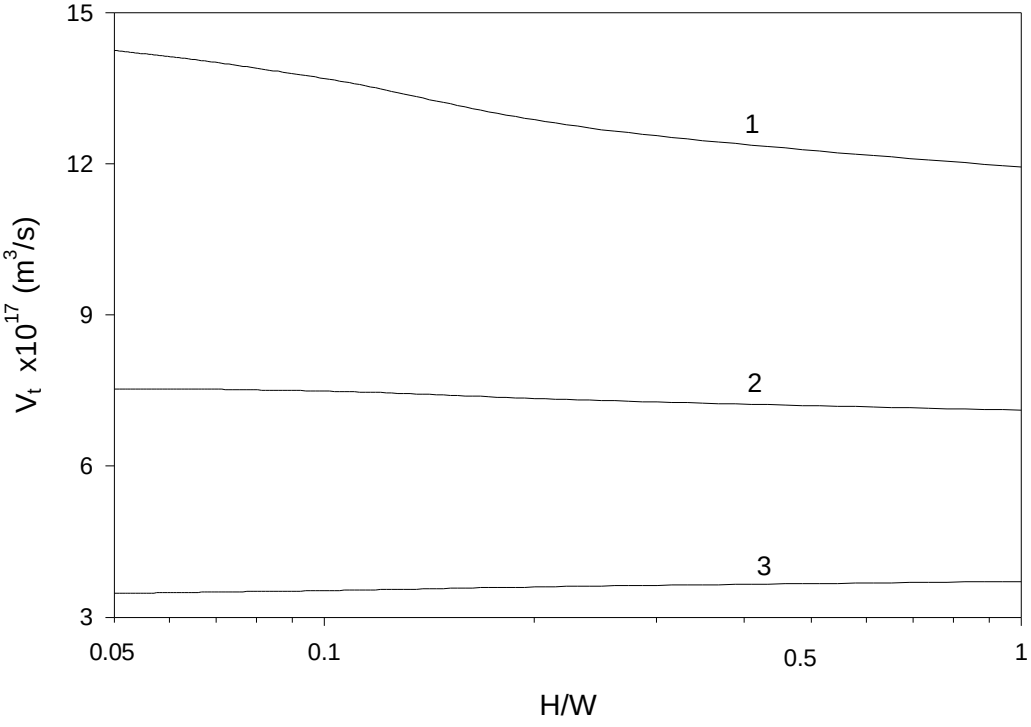

Fig.5a. Variation of volumetric flow rate V_t as a function of aspect ratio H/W at various ionic strength I and membrane thickness d for the case of Fig.4. Curve 1, $d=D_h/40$; Curve 2, $d=D_h/20$; Curve 3, $d=D_h/10$. Key: same as Fig.3 ($I=10^{-3}$ M).

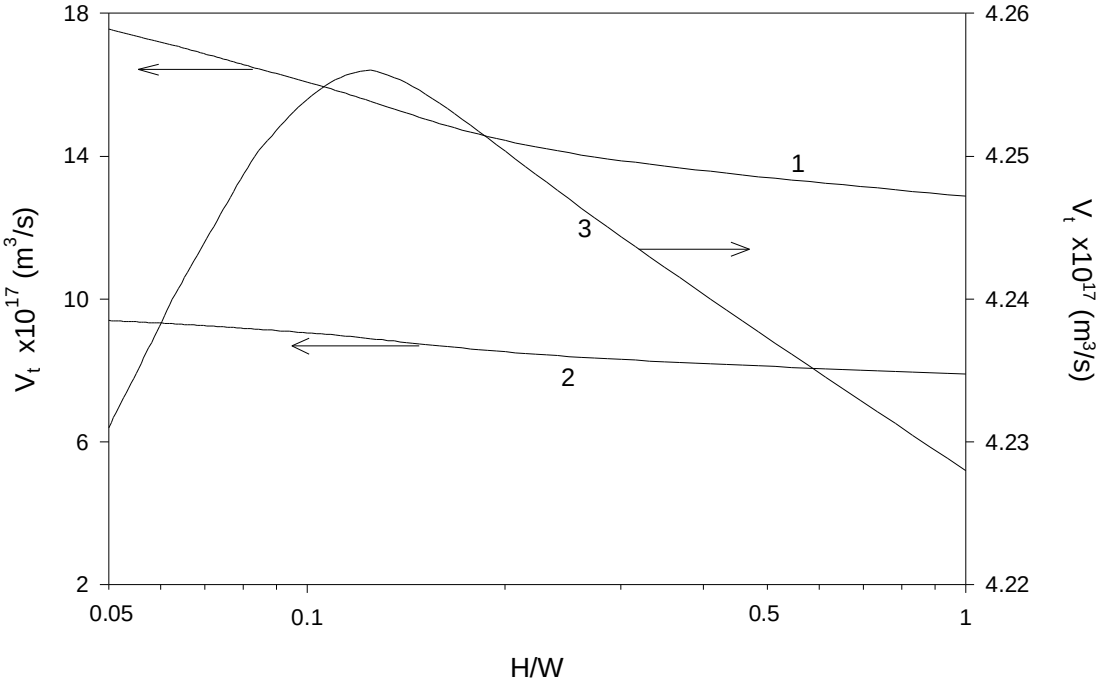

Fig.5b. Variation of volumetric flow rate V_t as a function of aspect ratio H/W at various ionic strength I and membrane thickness d for the case of Fig.4. Curve 1, $d=D_h/40$; Curve 2, $d=D_h/20$; Curve 3, $d=D_h/10$. Key: same as Fig.3 (I=5.5x10^{-4} M).

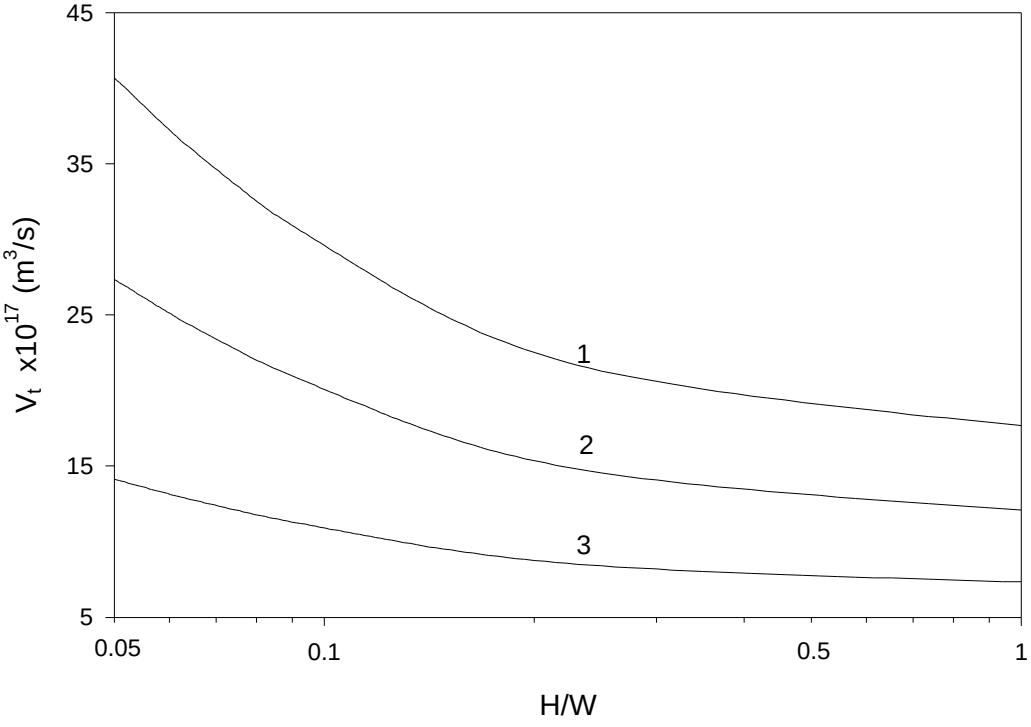

Fig.5c. Variation of volumetric flow rate V_t as a function of aspect ratio H/W at various ionic strength I and membrane thickness d for the case of Fig.4. Curve 1, $d=D_h/40$; Curve 2, $d=D_h/20$; Curve 3, $d=D_h/10$. Key: same as Fig.3 ($I=10^{-5}$ M).

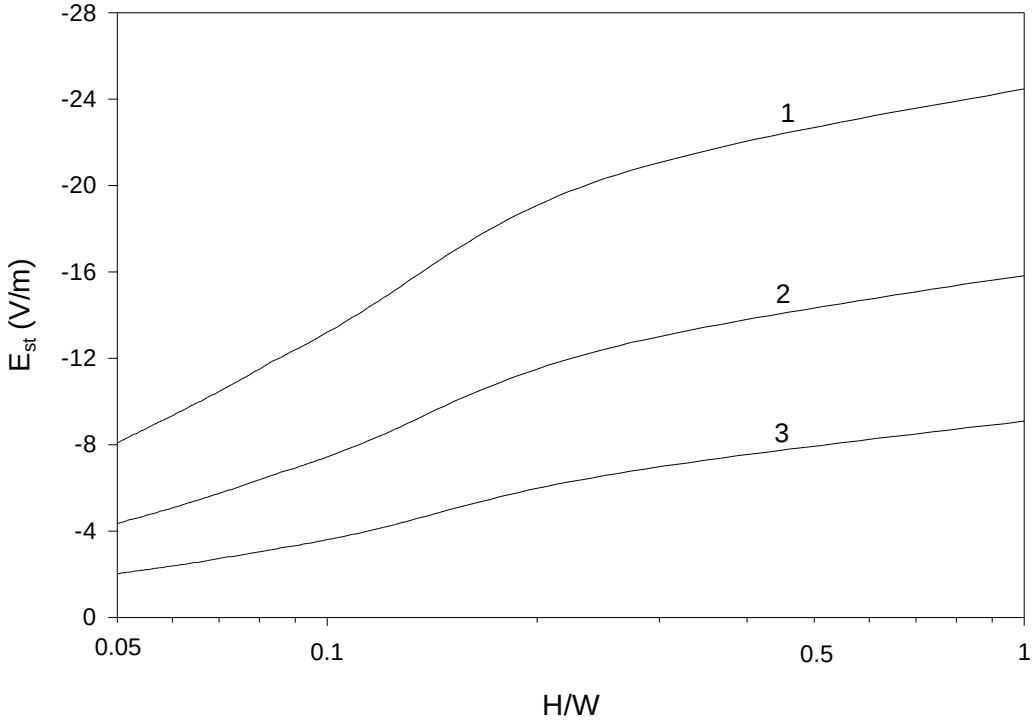

Fig.6a. Variation of streaming potential E_{st} as a function of aspect ratio H/W at various ionic strength I and membrane thickness d for the case $D_h=10^{-6}$ m and $P=10^7$ N/m^3. Curve 1, $d=D_h/40$; Curve 2, $d=D_h/20$; Curve 3, $d=D_h/10$. Key: same as Fig.3 ($I=10^{-3}$ M).

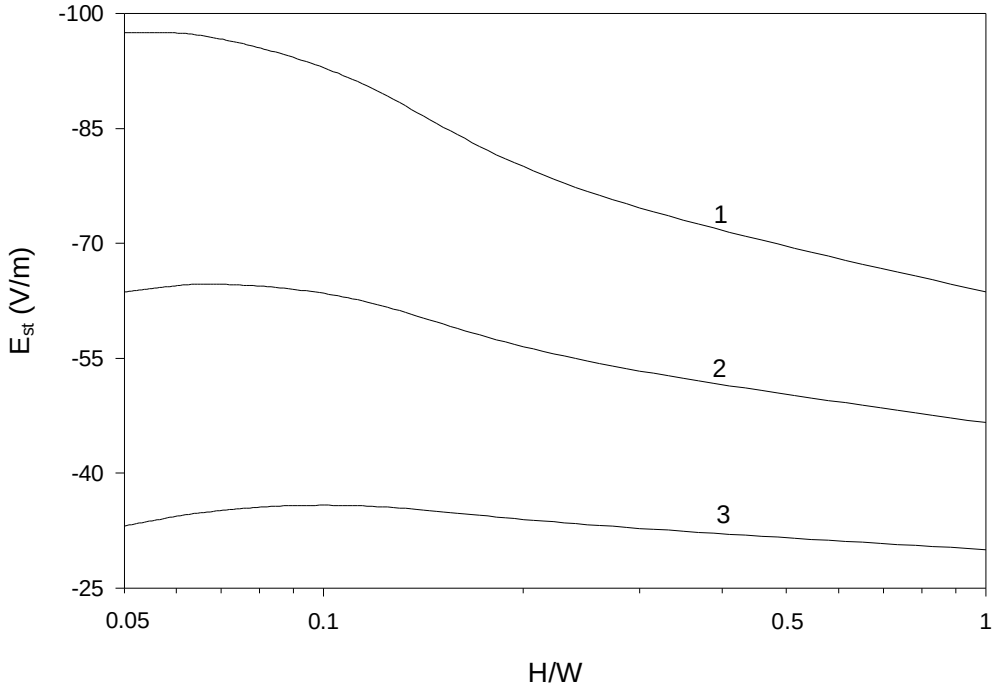

Fig.6b. Variation of streaming potential E_{st} as a function of aspect ratio H/W at various ionic strength I and membrane thickness d for the case $D_h=10^{-6}$ m and $P=10^7$ N/m^3. Curve 1, $d=D_h/40$; Curve 2, $d=D_h/20$; Curve 3, $d=D_h/10$. Key: same as Fig.3 ($I=10^{-4}$ M).

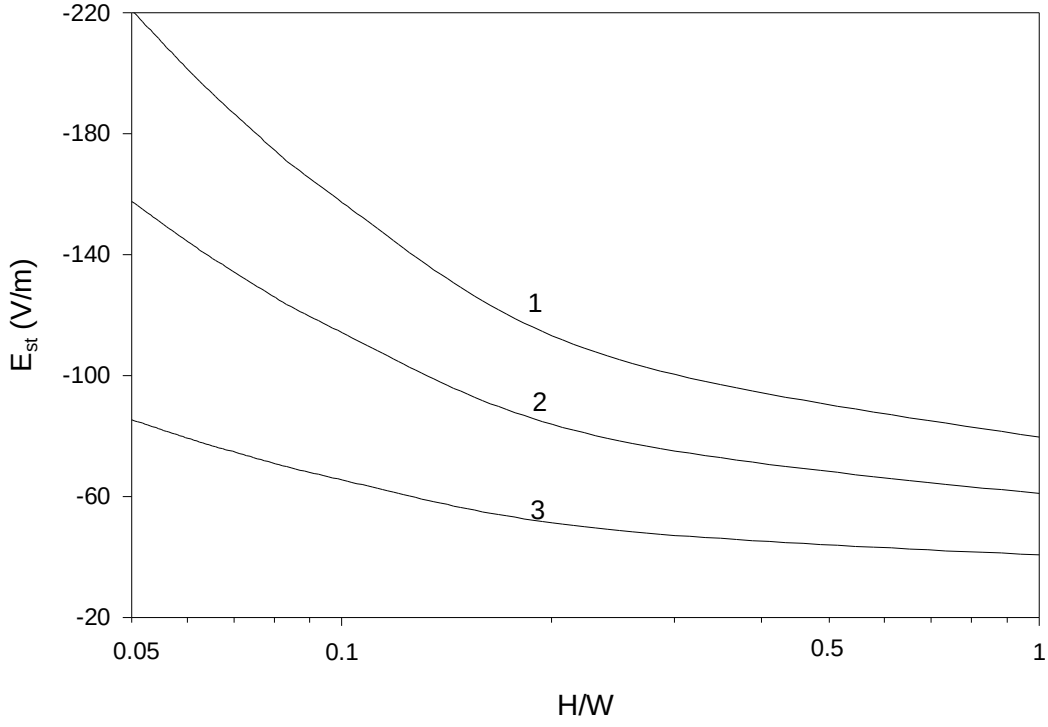

Fig.6c. Variation of streaming potential E_{st} as a function of aspect ratio H/W at various ionic strength I and membrane thickness d for the case $D_h=10^{-6}$ m and $P=10^7$ N/m^3. Curve 1, $d=D_h/40$; Curve 2, $d=D_h/20$; Curve 3, $d=D_h/10$. Key: same as Fig.3 ($I=10^{-5}$ M).

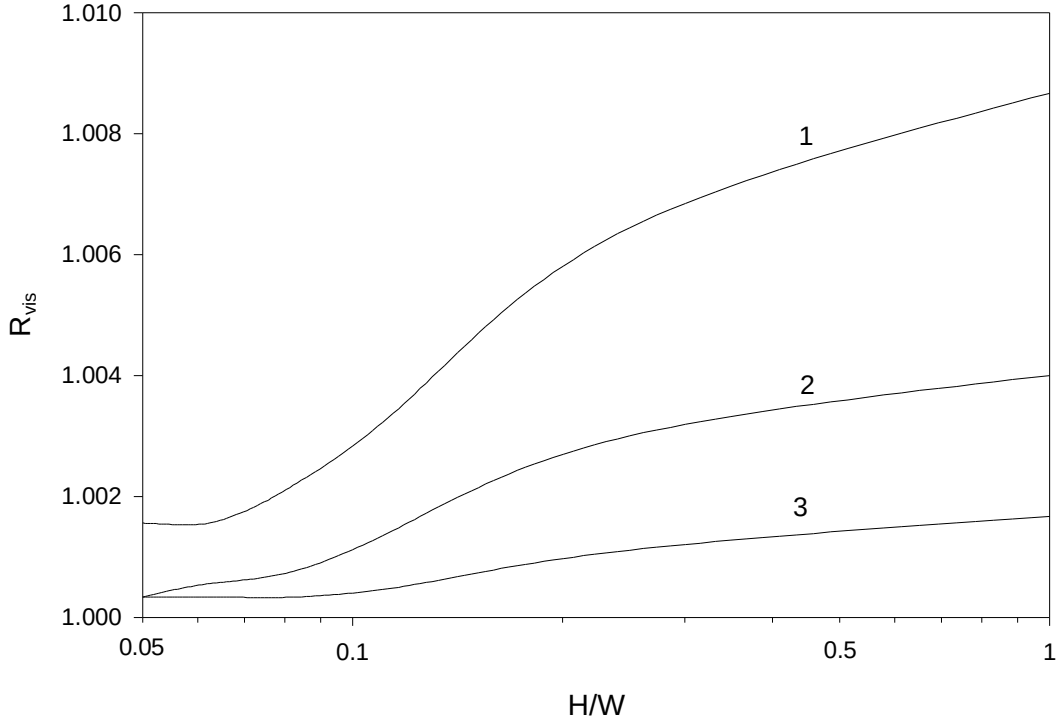

Fig.7a. Variation of viscosity ratio R_{vis} as a function of aspect ratio H/W at various ionic strength I and membrane thickness d for the case of Fig.6. Curve 1, $d=D_h/40$; Curve 2, $d=D_h/20$; Curve 3, $d=D_h/10$. Key: same as Fig.3 ($I=10^{-3}$ M).

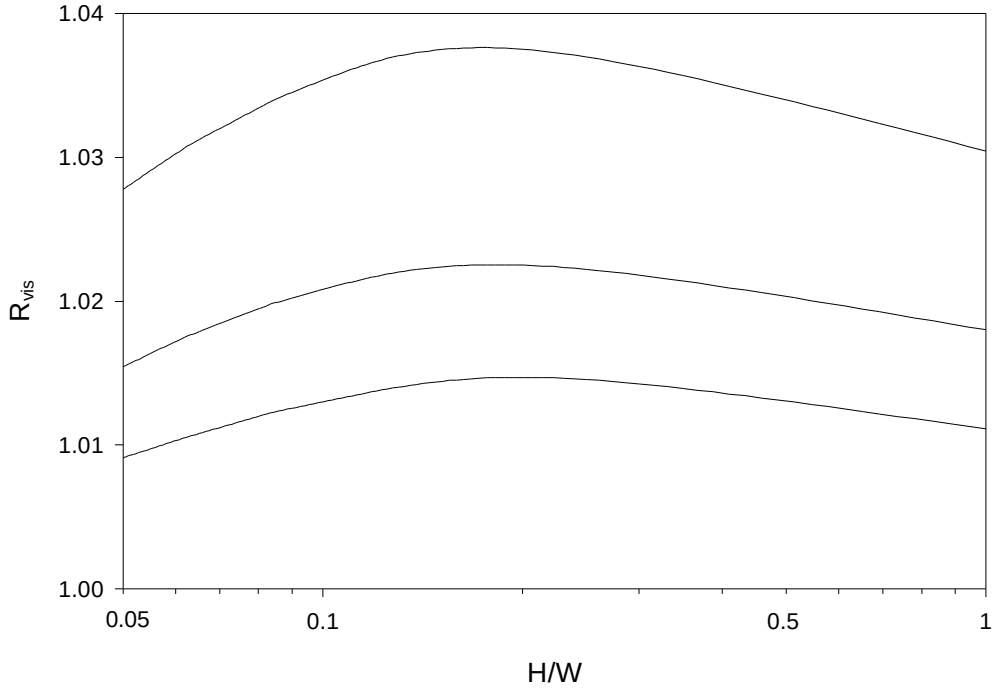

Fig.7b. Variation of viscosity ratio R_{vis} as a function of aspect ratio H/W at various ionic strength I and membrane thickness d for the case of Fig.6. Curve 1, $d=D_h/40$; Curve 2, $d=D_h/20$; Curve 3, $d=D_h/10$. Key: same as Fig.3 ($I=10^{-4}$ M).

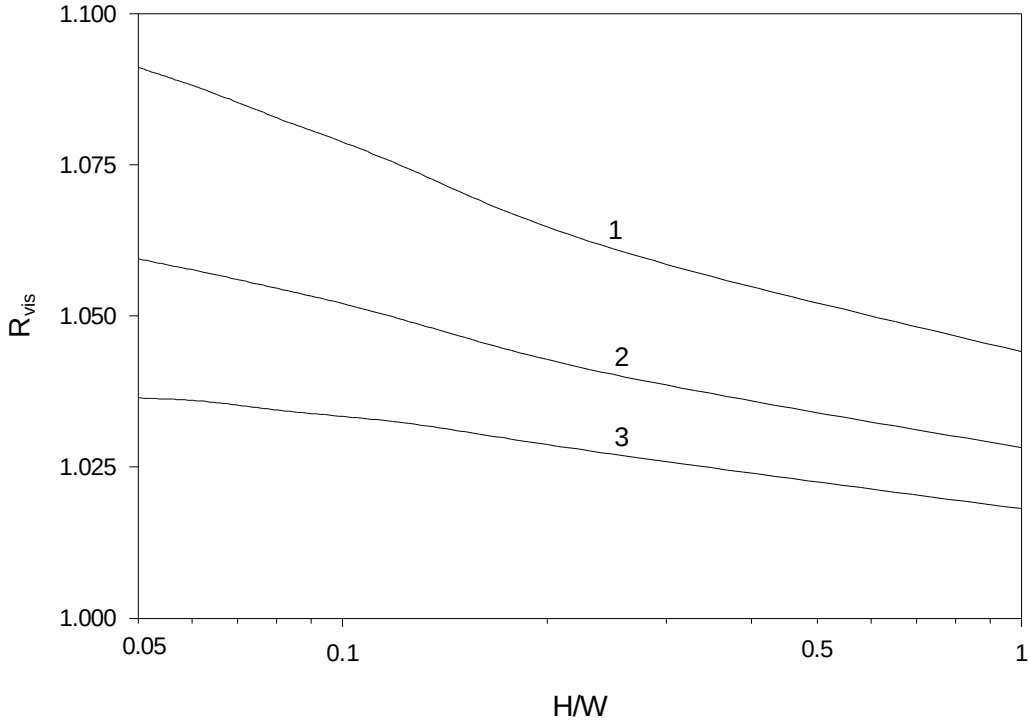

Fig.7c. Variation of viscosity ratio R_{vis} as a function of aspect ratio H/W at various ionic strength I and membrane thickness d for the case of Fig.6. Curve 1, $d=D_h/40$; Curve 2, $d=D_h/20$; Curve 3, $d=D_h/10$. Key: same as Fig.3 ($I=10^{-5}$ M).

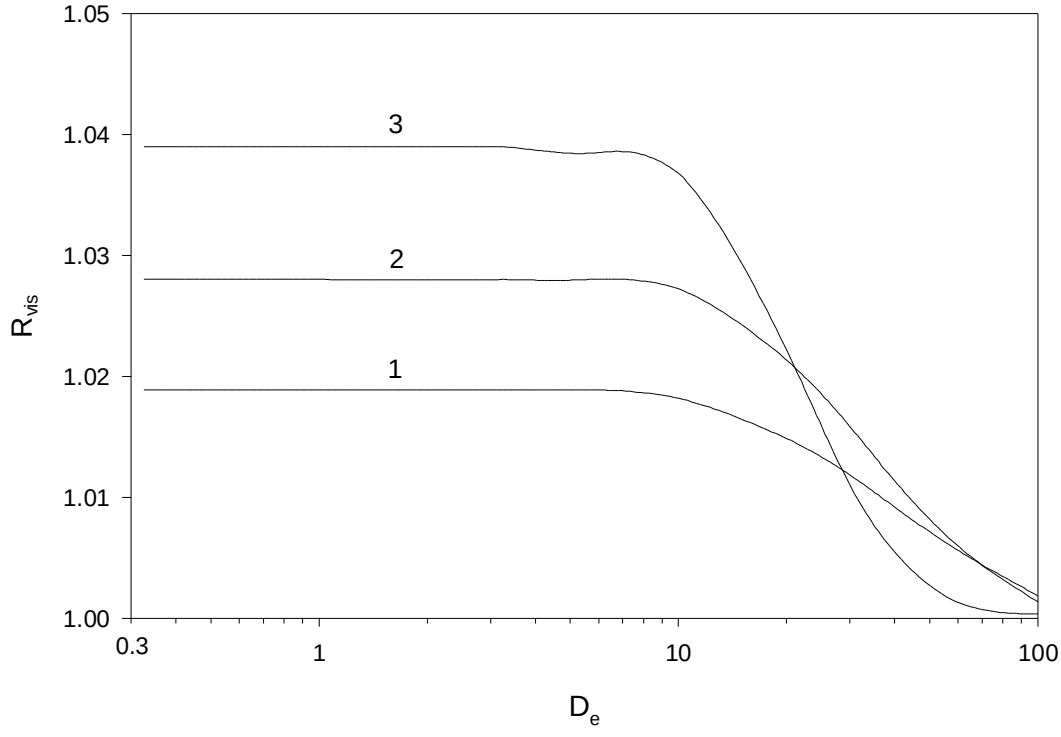

Fig.8a. Variation of viscosity ratio R_{vis} as a function of electrokinetic diameter D_e at various hydraulic diameter D_h and aspect ratio H/W for the case $d=D_h/10$ and $P=10^7$ N/m^3. Curve 1, H/W=1; Curve 2, H/W=1/4; Curve 3, H/W=1/20. Key: same as Fig.3 ($D_h=10^{-6}$ m).

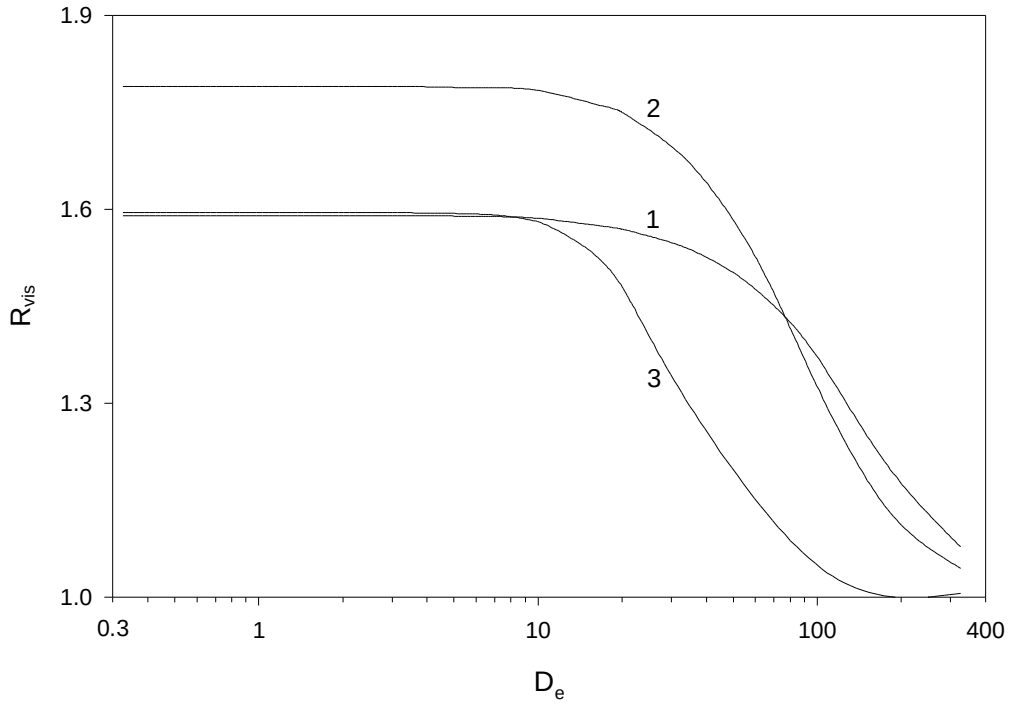

Fig.8b. Variation of viscosity ratio R_{vis} as a function of electrokinetic diameter D_e at various hydraulic diameter D_h and aspect ratio H/W for the case $d=D_h/10$ and $P=10^7$ N/m^3. Curve 1, H/W=1; Curve 2, H/W=1/4; Curve 3, H/W=1/20. Key: same as Fig.3 ($D_h=10^{-7}$ m).

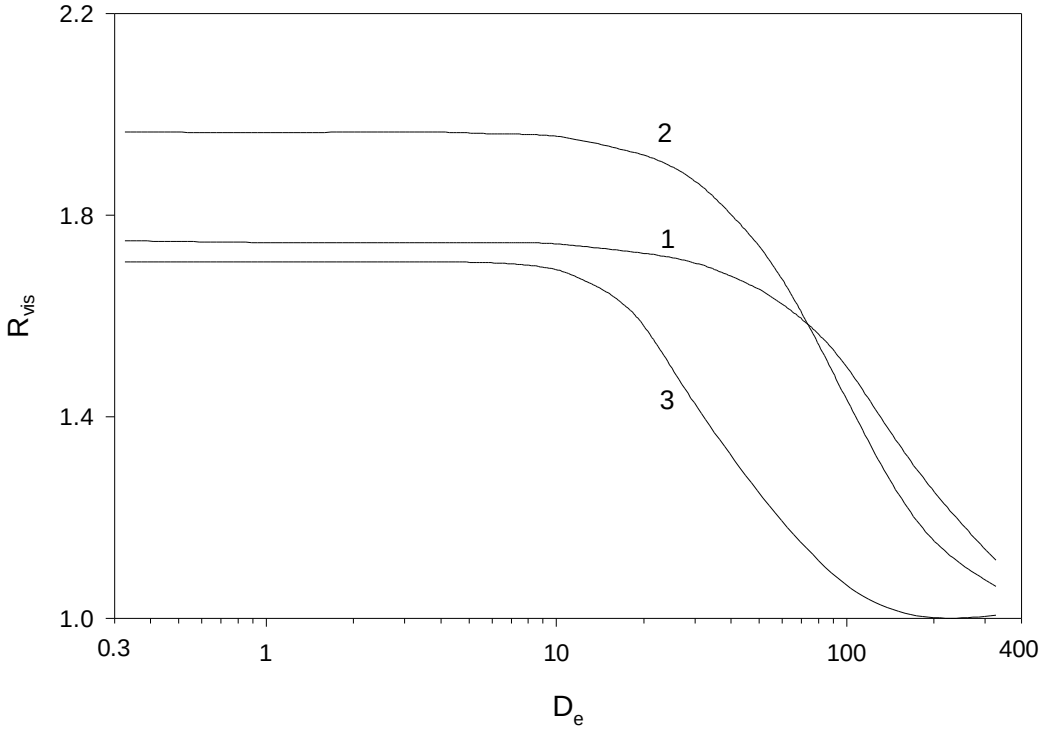

Fig.8c. Variation of viscosity ratio R_{vis} as a function of electrokinetic diameter D_e at various hydraulic diameter D_h and aspect ratio H/W for the case $d=D_h/10$ and $P=10^7$ N/m^3. Curve 1, H/W=1, Curve 2, H/W=1/4; Curve 3, H/W=1/20. Key: same as Fig.3 ($D_h=10^{-8}$ m).

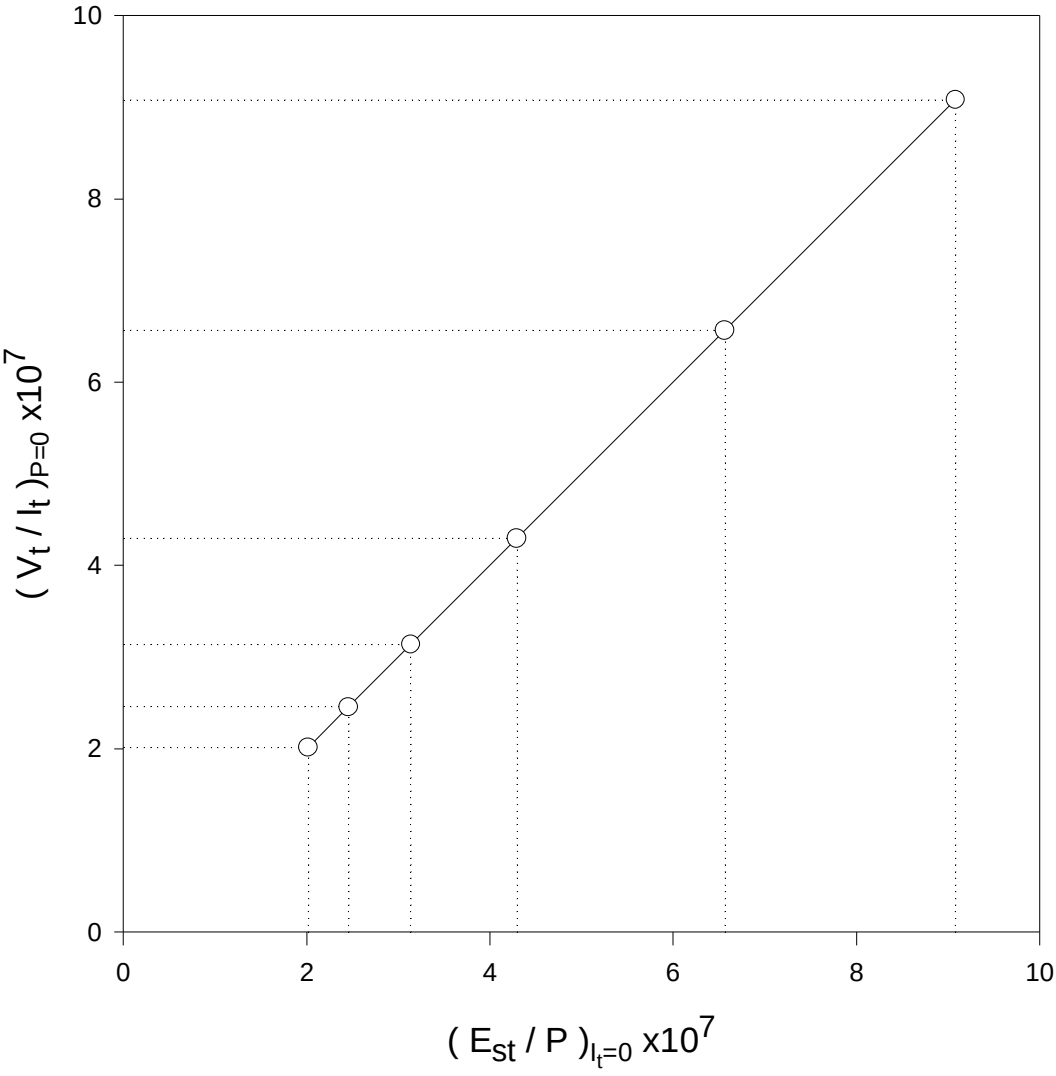

Fig.9. Variation of $(V_t/I_t)_{P=0}$ as a function of $(E_{st}/P)_{It=0}$ at various aspect ratio H/W (1, 1/4, 1/8, 1/12, 1/16, and 1/20, from top to down). Parameters used are $D_h=10^{-6}$ m, $I=10^{-3}$ M, $d=D_h/10$. Key: same as Fig.3.

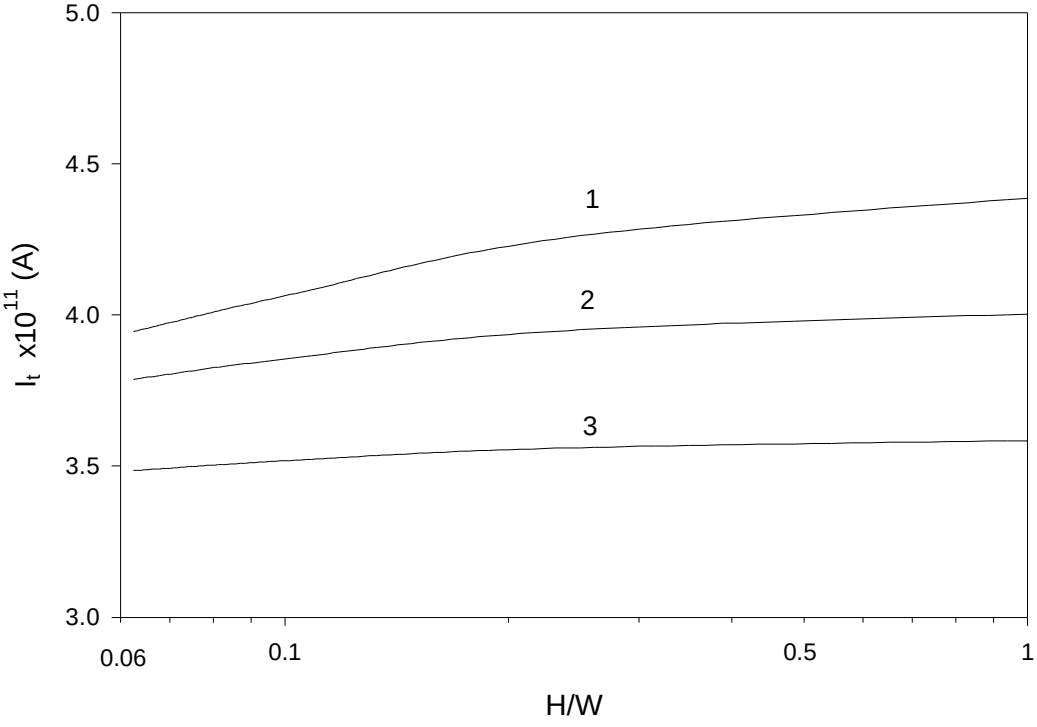

Fig.10a. Variation of total current I_t as a function of aspect ratio H/W at various ionic strength I and membrane thickness d. Parameters used are E_z=1000 V/m, P=0 N/m^3 and D_{hc}=10^{-6} m. Curve 1, d_c=D_{hc}/40; Curve 2, d_c=D_{hc}/20; Curve 3, d_c=D_{hc}/10, D_{hc} is the diameter of a cylindrical channel covered by a circular membrane of thickness d_c. Key: same as Fig.3 (I=10^{-3} M).

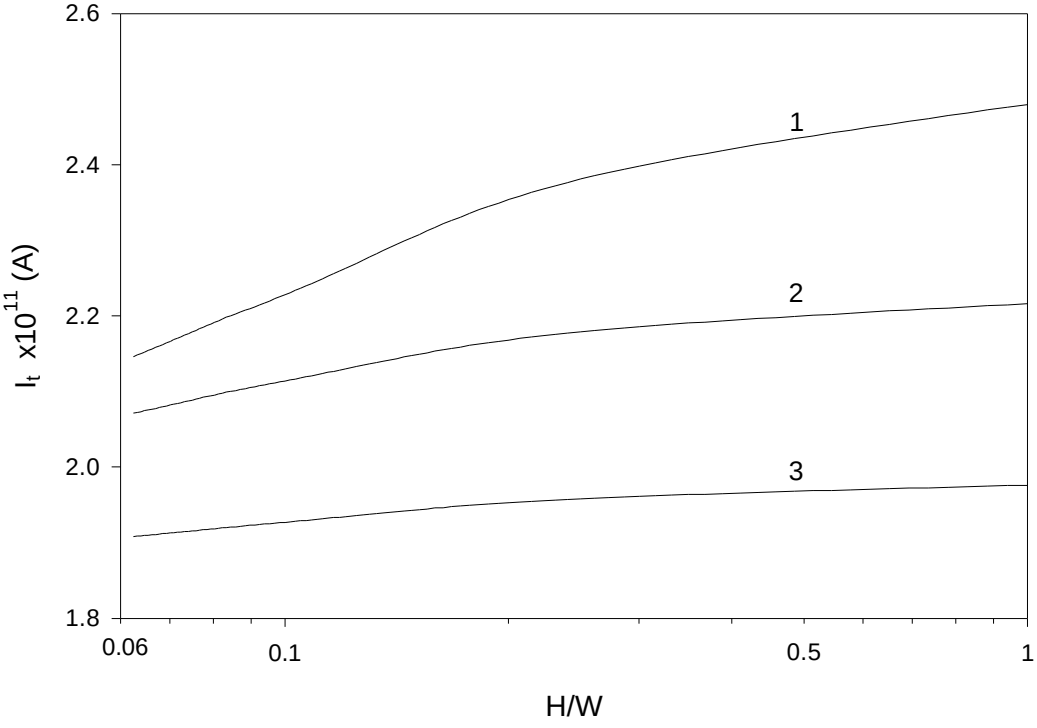

Fig.10b. Variation of total current I_t as a function of aspect ratio H/W at various ionic strength I and membrane thickness d. Parameters used are E_z=1000 V/m, P=0 N/m^3 and D_{hc}=10^{-6} m. Curve 1, d_c=D_{hc}/40; Curve 2, d_c=D_{hc}/20; Curve 3, d_c=D_{hc}/10, D_{hc} is the diameter of a cylindrical channel covered by a circular membrane of thickness d_c. Key: same as Fig.3 (I=10^{-4} M).

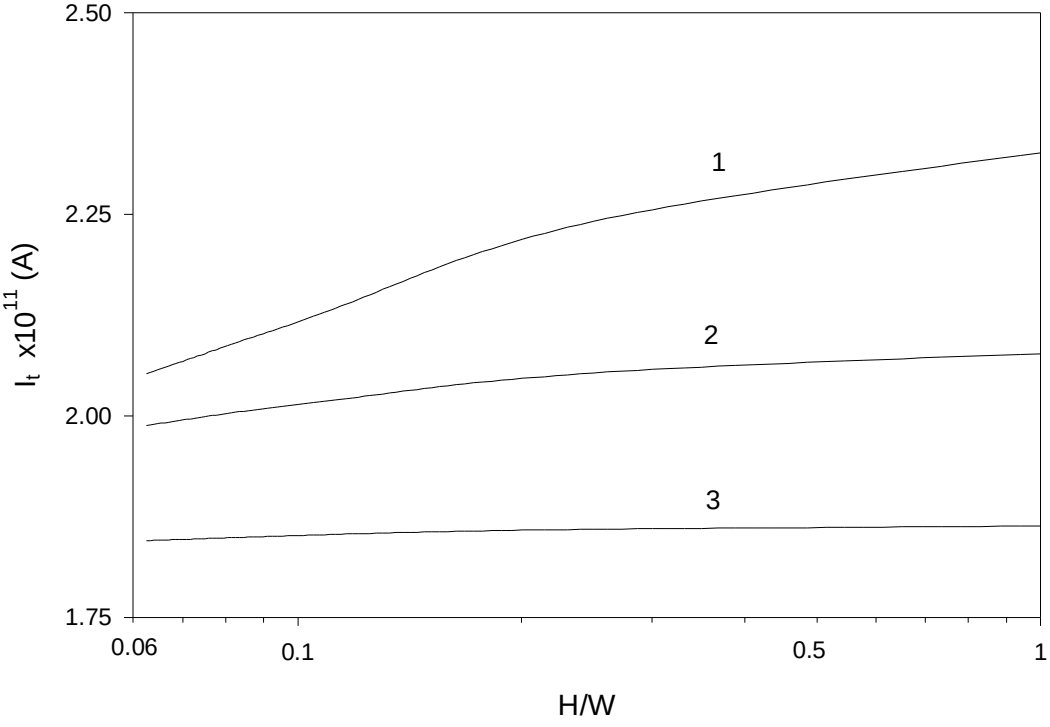

Fig.10c. Variation of total current I_t as a function of aspect ratio H/W at various ionic strength I and membrane thickness d. Parameters used are E_z=1000 V/m, P=0 N/m^3 and D_{hc}=10^{-6} m. Curve 1, d_c=D_{hc}/40; Curve 2, d_c=D_{hc}/20; Curve 3, d_c=D_{hc}/10, D_{hc} is the diameter of a cylindrical channel covered by a circular membrane of thickness d_c. Key: same as Fig.3. (I=10^{-5} M).